Mapping Hydration Water Molecules in the HIV-1 Protease/DMP323 Complex in Solution by NMR Spectroscopy[†]

Yun-Xing Wang,[‡] Darón I. Freedberg,[‡] Stephan Grzesiek,[§] Dennis A. Torchia,*[,‡] Paul T. Wingfield,[∥] Joshua D. Kaufman,[∥] Stephen J. Stahl,[∥] Chong-Hwan Chang,[⊥] and C. Nicholas Hodge[⊥]

Molecular Structural Biology Unit, NIDR, Laboratory of Chemical Physics, NIDDK, and Protein Expression Laboratory, NIAMS, National Institutes of Health, Bethesda, Maryland 20892-4320, and Department of Chemical and Physical Science, The DuPont Merck Pharmaceutical Company, Wilmington, Delaware 19880-0353

Received May 6, 1996; Revised Manuscript Received July 12, 1996[⊗]

ABSTRACT: A tetrahedrally hydrogen-bonded structural water molecule, water 301, is seen in the crystal structure of nearly every HIV-1 protease/inhibitor complex. Although the urea oxygen of the designed inhibitor, DMP323, mimics and replaces water 301, other water molecules are seen in the protease/DMP323 crystal structure. As a first step toward understanding how water molecules may contribute to inhibitor potency and specificity, we have recorded water−NOESY and water−ROESY spectra of the protease/DMP323 complex. Cross relaxation rates derived from these spectra, together with interproton distances calculated from the crystal structure of the complex, were used to classify the exchange cross peaks as follows: (A) a direct NOE with a water proton, (B) an indirect NOE with water through a labile protein proton, and (C) direct exchange of an amide proton with water. Type A and B cross peaks were analyzed using three models of water dynamics: (1) two-site exchange, with water molecules randomly hopping between bound and free states, (2) bound water with internal motion, and (3) free diffusion. Using the two-site exchange model to analyze the relaxation data of the type A cross peaks, it was found that the water molecules had short residence times, ca. 500 ps, in contrast with the >9 ns residence time estimated for water 301 in the protease/P9941 complex [Grzesiek et al. (1994) *J. Am. Chem. Soc. 116*, 1581−1582]. The NMR data are consistent with the X-ray observation that two symmetry-related water molecules, waters 422 and 456, are bound at the DMP323 binding site. Hence, these water molecules may help to stabilize the structure of the complex. Finally, it was found that three buried and hydrogen-bonded Thr hydroxyl protons were in slow exchange with solvent. In contrast, it was found that the DMP323 H4/H5 hydroxyl protons and the Asp25/125 carboxyl protons, which form a buried hydrogen-bonded network at the catalytic site of the protease, are in rapid exchange with solvent, suggesting that solvent can penetrate into the buried protein/inhibitor interface on the millisecond to microsecond time scale.

The HIV-1[1] protease is a homodimeric enzyme that is indispensable for maturation of the AIDS virus. This protein is therefore a primary target for inhibitory drug therapy (Wlodawer & Erickson, 1993; Lam et al., 1994). In the crystal structure of nearly every HIV-1 protease/inhibitor complex, a tetrahedrally coordinated and buried structural water molecule, water 301, bridges the flaps of the protein to the inhibitor by accepting two hydrogen bonds from the NH groups of Ile50/Ile150 and donating two hydrogen bonds to CO groups of the inhibitor P1/P2′ sites (Wlodawer & Erickson, 1993). Water 301 has been observed in solution (Grzesiek et al., 1994), showing that it is not an artifact of crystallization. In solution, water 301 was found to have a long residence time, greater than ca. 10^{-8} s (Grzesiek et al., 1994), consistent with the observation that it is hydrogen bonded and solvent inaccessible in the crystalline state (Wlodawer & Erickson, 1993).

In contrast with HIV-1 protease/inhibitor structures, mammalian protease/inhibitor structures are unable to accommodate a structural water molecule analogous to water 301 (Wlodawer & Erickson, 1993). This observation has stimulated the design of a novel series of cyclic urea inhibitors (Lam et al., 1994) in which the urea oxygen replaces and mimics the function of the water 301 oxygen. In addition to improving inhibitor specificity, adding the water 301 oxygen mimic to the rigid urea ring of the inhibitor was expected to enhance the entropic contribution to complex formation and thereby increase inhibitor affinity for the protease. In accord with these expectations, the cyclic urea inhibitors have been found to be highly potent and specific inhibitors of the protease (Lam et al., 1994). The urea moiety of one such inhibitor, DMP323 (Figure 1), $K_i = 0.27$ nM, has been shown to replace and mimic the role of water 301 both in the crystalline state, Figure 2 (Lam et al., 1994), and in solution (Grzesiek et al., 1994).

[†] This work was supported by the AIDS Targeted Antiviral Program of the Office of the Director of the National Institutes of Health.

* Corresponding author: Bldg 30, Room 132, NIDR, NIH, Bethesda, MD 20892. Phone: 301-496-5750. FAX: 301-402-1512.

[‡] Molecular Structural Biology Unit, NIDR.

[§] Laboratory of Chemical Physics, NIDDK.

[∥] Protein Expression Laboratory, NIAMS.

[⊥] The DuPont Merck Pharmaceutical Co.

[⊗] Abstract published in *Advance ACS Abstracts,* September 1, 1996.

[1] Abbreviations: NMR, nuclear magnetic resonance; NOESY, nuclear Overhauser effect spectroscopy; ROESY, nuclear Overhauser effect spectroscopy in the rotating frame; HSQC, heteronuclear single-quantum correlation spectroscopy; DMP323, (4*R*,5*S*,6*S*,7*R*)-hexahydro-5,6-dihydroxy-1,3-bis[[4-(hydroxymethyl)phenyl]methyl]-4,7-bis-(phenylmethyl)-2*H*-1,3-diazepin-2-one; HIV-1, human immunodeficiency virus type 1.

S0006-2960(96)01076-8 CCC: $12.00

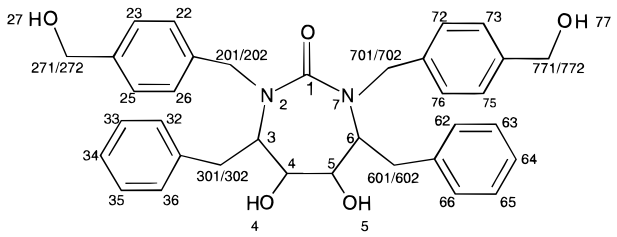

FIGURE 1: Chemical structure of DMP323. The numbering scheme is the same as in Yamazaki et al. (1996). Note that there are four hydroxyl groups in the molecule.

Although water 301 is not found in the protease/DMP323 complex, numerous other water molecules are observed in the crystal structure of this complex, as well as in the structures of the protease complexed with other potent inhibitors (Baldwin et al., 1995). A better understanding of the interactions between water molecules and the protease, complexed with its ligands, could facilitate design of more potent inhibitors, and the goal of this investigation is to identify water molecules that bind to the protease/DMP323 complex in solution.

Recently it has been shown that NMR techniques are well suited to identify hydration water molecules associated with proteins and nucleic acids in solution (Otting & Wüthrich, 1989; Clore et al., 1990; Otting et al., 1991; Kriwacki et al., 1993). These experiments provide the resolution and sensitivity needed to identify sequentially assigned protein protons that have NOE/ROE interactions with nearby water protons. In favorable cases, measurement of NOE/ROE cross relaxation rates can be used to estimate residence times of hydration water molecules (Otting et al., 1991). Although NOE/ROE interactions with labile protons, such as hydroxyl protons, can limit measurement of hydration water lifetimes, the experiments can yield estimates of exchange lifetimes of buried hydroxyl protons such as those at the active site of the complex, thus providing information about the time scale that these "solvent-inaccessible" regions of the protease/inhibitor structure make contact with solvent.

MATERIALS AND METHODS

Sample Preparation. The HIV-1 protease sequence is that of the HXB2 isolate with Cys to Ala substitutions at positions 67 and 95. The fully $^{13}C/^{15}N$-labeled recombinant HIV-1 protease was prepared and purified as described previously (Yamazaki et al., 1996). A solution of the purified protein, containing a 5-fold molar excess of DMP323, was dialyzed overnight against 4 L of buffer containing 50 mM NaOAc, pH 4.5, and the protein/DMP323 complex was concentrated to about 0.9 mL in an Amicon Centriprep-10. The NMR sample solution was prepared by exchanging the protonated buffer, pH 4.5, against a total of 10 volumes of 50 mM NaOAc-d_3, pH 5.2, and 10% D_2O in an Amicon Centriprep-10. The sample volume was $\sim$240 μL in a 5 mm Shigemi NMR tube (Shigemi, Inc., Allison Park, PA), and the sample concentration was ca. 1.2 mM, determined by absorption at 280 nm, with $\epsilon \approx 0.85$ mg/OD. The top of the Shigemi tube was tightly wrapped with Teflon tape and Parafilm.

NMR Spectroscopy. NMR spectra were recorded at 34 °C on a Bruker AMX500 spectrometer equipped with a carbon-optimized, *z*-gradient, triple-resonance ($^1H-^{13}C-^{15}N$) probe. Signal assignments (^1H, ^{13}C, and ^{15}N) are essentially the same as for the C95A protease/DMP323 complex, published elsewhere (Yamazaki et al., 1994a).

NOE and ROE interactions between water and protein protons attached to ^{15}N or ^{13}C were detected by recording 2D versions of NOESY or ROESY heteronuclear single-quantum coherence (HSQC) spectra (Grzesiek & Bax, 1993a,b), called herein WNOESY and WROESY spectra, respectively. These experiments offer higher sensitivity than their 3D counterparts because of their lower dimensionality and because water *z*-magnetization is kept nearly at equilibrium (Grzesiek & Bax, 1993a,b). Spectra are recorded in an interleaved mode, with the water magnetization aligned either parallel ($+z$) or antiparallel ($-z$) to the magnetization of all other ^1H spins, during the NOE (ROE) mixing period. The difference spectrum contains NOE (ROE) cross peaks between water protons and protein protons, while the sum spectrum has the appearance of an HSQC spectrum. Protein and inhibitor protons that are not attached to ^{13}C and resonate near water also yield NOE (ROE) signals. These signals are identified by a "control experiment" (Grzesiek et al., 1994) that selectively attenuates water-derived cross peaks ca. 20-fold.

WNOESY and WROESY spectra were recorded with respective mixing times of 100 and 50 ms. A total of 256 FIDs (128 hypercomplex points) were recorded for both the amide, $^1H-^{15}N$, and the aliphatic, $^1H-^{13}C$, spectra with ^1H detection times of 60 and 100 ms, respectively. The data were zero-filled to 1024 points in F_2 and 256 points in F_1. For the amide spectra, the carrier was set at 4.69 ppm in the ^1H dimension (F_2) and 120.0 ppm in ^{15}N dimension (F_1), with spectral widths of 8064.5 Hz in F_2 and 2000.0 Hz in F_1. The data were multiplied by a Lorentz-to-Gauss window function with a Lorentzian width of -7.0 Hz and Gaussian width of 20.0 Hz before Fourier transformation in both F_1 and F_2. For the aliphatic spectra, the carrier was set at 4.69 ppm in F_2 and 125.76 ppm in F_1 (^{13}C), with spectral widths of 8065 Hz in F_2 and 8333 Hz in F_1. The data were multiplied by a 60°-shifted-sine-squared window function in F_2 and a 60°-shifted-sine window function in F_1 before Fourier transformation. Data were processed on SUN Sparc stations using the program nmrPipe (Delaglio et al., 1995).

Relaxation rates in the laboratory ($\rho_1 + k_n$) and rotating ($\rho_2 + k_r$) frames were measured as described previously (Grzesiek & Bax, 1993b). The peak intensities in the sum spectra (equivalent to the diagonal peaks in a normal NOESY/ROESY spectrum) were measured using the program PIPP (Garrett et al., 1991), and $\rho_1 + k_n$ and $\rho_2 + k_r$ were then calculated using a two-point approximation

$$\rho + k = [\ln(I_1/I_2)]/(t_2 - t_1) \qquad (1)$$

where I_1 and I_2 are the intensities measured with delays of t_1 (2 ms) and t_2 (50 ms). Simulations of the Ayant diffusion model (Ayant et al., 1977) were performed using Mathematica, Wolfram Research, Inc., Champaign, IL.

THEORETICAL BACKGROUND

Grzesiek and Bax (1993b) have derived equations relating cross relaxation rates, $\sigma_{NOE}/\sigma_{ROE}$, to normalized signal intensities ξ_{NOE}/ξ_{ROE} measured in WNOESY/WROESY experiments. In a simplified form (assuming that water and protein magnetization recover fully after each scan, that the rate of chemical exchange with water is much less than σ_{NOE},

and that $\rho_1 \gg \sigma_{NOE}$ and $\rho_2 \gg \sigma_{ROE}$), these equations are

$$\sigma_{NOE}(t) = -\xi_{NOE}(t)\rho_1/[1 - \exp(-\rho_1 t)] \quad (2)$$

$$\sigma_{ROE}(t) = -\xi_{ROE}(t)\rho_2/[\exp(\rho_2 t) - 1] \quad (3)$$

where ρ_1 is the protein proton relaxation (spin flip) rate in the laboratory frame, ρ_2 is the protein proton relaxation rate in the rotating frame, ξ_{NOE} or ξ_{ROE} is equal to the ratio I^-/I^+, where I^- and I^+ are the signal intensities in the difference and sum WNOESY or WROESY spectra, respectively. The signal-to-noise ratio is usually smaller in the WROESY difference spectrum because the spin-locked protein protons decay as $\exp(-\rho_2 t)$. For a typical mixing time in the 50−100 ms range, $\rho t > 1$, and the signal-to-noise ratio of each experiment is roughly proportional to σ/ρ.

Using the measured values of ξ and ρ, and taking into account the partial recovery of water magnetization at the beginning of each scan (Grzesiek & Bax, 1993b), the exact forms of eqs 2 and 3 were used to calculate the cross relaxation rates σ_{NOE} and σ_{ROE}. These rates are related to the power spectral density function, $J(\omega)$, describing the dynamics of hydration water molecules according to

$$\sigma_{NOE} = -d[6J(2\omega) - J(0)] \quad (4)$$

$$\sigma_{ROE} = d[2J(0) + 3J(\omega)] \quad (5)$$

where $d = (1/40)/(h\gamma^2/\pi)^2$, h is Planck's constant, γ is the proton gyromagnetic ratio, and ω is the proton Larmor precession frequency. The explicit form of $J(\omega)$ depends upon the specific model used to describe the dynamics of the internuclear vector, **r**, joining the protons in the protein and hydration water molecules.

In the case of a bound water molecule undergoing exchange with bulk water, the spectral density function has the form

$$J(\omega) = \frac{1}{r^6}\frac{\tau_c}{(1 + \omega^2\tau_c^2)} \quad (6)$$

where τ_c is the correlation time and r is the internuclear distance between the water proton and protein proton. Note that two distinct types of motion modulate the dipolar interaction. The first is two-state spin exchange, similar to that described by Abragam (1961) in his discussion of scalar relaxation of the first kind, with a correlation time τ_{re}. It is assumed that in the bound state the water molecule has a dipolar interaction with the protein, whereas in the free state it does not, resulting in a modulation of the dipolar interaction. The second type of motion is reorientation of **r**, with correlation time τ_o, due to rotational diffusion of the protein. In eq 6, the correlation time τ_c equals τ_{re} provided that $\tau_{re} \ll \tau_o$; conversely, τ_c equals τ_o when $\tau_{re} \gg \tau_o$, as might be expected for a tightly bound interior water molecule. When τ_{re} and τ_o are comparable, $1/\tau_c$ is approximately equal to $1/\tau_{re} + 1/\tau_o$, provided that relaxation due to exchange and overall protein tumbling are not correlated.

If the orientation of **r** is also modulated by internal motion, the formalism of Lipari and Szabo (1982) leads to the following generalization of eq 6

$$J(\omega) = \frac{1}{r^6}\left[\frac{S^2\tau_c}{1 + \omega^2\tau_c^2} + \frac{1 - S^2}{1 + \omega^2\tau^2}\right] \quad (7)$$

where S^2 is the generalized order parameter, $1/\tau = 1/\tau_c + 1/\tau_{int}$, and τ_{int} is the effective correlation time of the internal motion of **r**. Although S^2 includes only the effect of fluctuations in the orientation of **r**, a generalization of eq 7 that takes account of fluctuations in the length of **r** is available (Lipari & Szabo, 1982).

Thus far it has been assumed that a particular water molecule resides close to a protein proton for a considerable period before instantaneously exchanging with another water molecule and rapidly diffusing away. The spectral density functions derived using this model do not apply when a continuum of water molecules diffuse in the vicinity of the protein proton. This case has been modeled assuming that the spins are attached to spheres undergoing rotational and translational diffusion (Ayant et al., 1977) with the result

$$J(\omega) = \frac{N_s}{24\pi D b}\sum_{l=0}^{\infty}(2l + 4)(2l + 3)(2l + 2)\left(\frac{\rho_I}{b}\right)^{2l} A_{l,l}(\omega) \quad (8)$$

where

$$A_{l,l}(\omega) = \mathrm{Re}\left\{\frac{1}{\nu_{l,l}^2}\left[\frac{1}{2l + 1} - \frac{l + 3}{\nu_{l,l}^2}\left(1 + \frac{l + 3}{\nu_{l,l}}\frac{K_{l+5/2}(\nu_{l,l})}{K_{l+3/2}(\nu_{l,l})}\right)^{-1}\right]\right\} \quad (9)$$

$$\nu_{l,l} = [i\omega\tau + l(l + 1)\tau D_p^r]^{1/2} \quad (10)$$

and N_s is the density of proton spins in bulk water, 0.067 Å^{-3} (Brüschweiler & Wright, 1994), K is the modified spherical Bessel function of the third kind, D is the sum of the translational diffusion coefficients of the protein and water molecules, and D_p^r is the rotational diffusion coefficient of the protein. As depicted in Figure 3, spin I represents a protein proton and spin S a water proton (the latter assumed to be at the center of the water molecule), b is the sum of the radii of the spheres representing the protein and water molecules, ρ_I is the distance between I and the center of the protein, $\Delta = b - \rho_I = r_{min}$, the distance of closest approach of the protein and water spins, and τ is defined as b^2/D. Because the diffusion coefficient of water, D_w^{tr}, is much larger than that of the protein, we expect that $D \approx D_w^{tr}$. The translational diffusion coefficient of water at 278 K is 1.2×10^{11} Å^2 s^{-1} (Gillen et al., 1972).

A comparison of the predictions of the exchange and Ayant models provides insight into the dependence of the cross relaxation rate upon (a) the distance between water and protein spins and (b) the residence time/diffusion coefficients of hydration water molecules. Plots of σ_{NOE}, σ_{ROE}, and their ratio, R_σ, vs τ_c (Figure 4), for the exchange model show that σ_{ROE} is a positive, increasing function of τ_c. In contrast, σ_{NOE} vanishes when $\omega_0\tau_c = \sqrt{5}/2$ (i.e., τ_c ca. 360 ps at 500 MHz) (Otting et al., 1991) and then becomes negative, attaining a value of $-\sigma_{ROE}/2$ in the slow motion limit. The value of τ_c can be determined from R_σ (Figure 5), except in the slow motion limit, $(\omega_0\tau_c)^2 \gg 1$, where R_σ is nearly independent of τ_c.

The situation is more complex in the presence of internal motion which modulates the orientation of **r**. Values of R_σ,

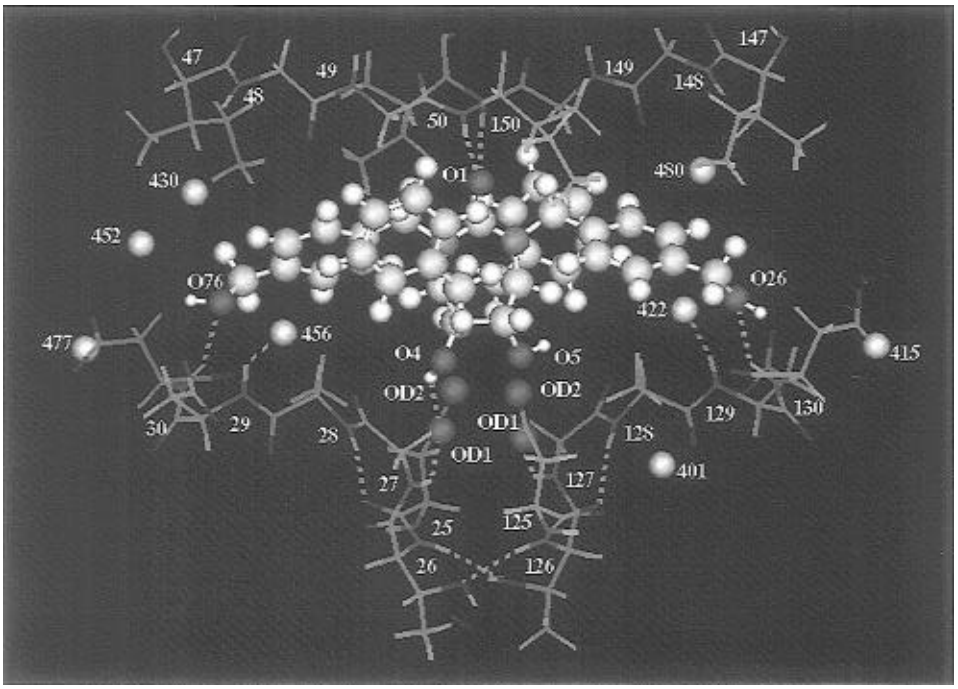

FIGURE 2: Quanta drawing of DMP323 (ball and stick) in the active site of the HIV-1 protease. Nearby water molecules observed in the crystal structure are shown as yellow spheres with identifying numbers. The DMP323 urea oxygen, O1, is located just beneath the I50/I150 amide protons from which it accepts hydrogen bond (indicated by gray broken lines). The hydroxyl groups at the bottom of the inhibitor, O4 and O5, form a hydrogen bond network (not drawn) with the nearby catalytic Asp25/125 carboxyl oxygens, OD1 and OD2 (Yamazaki et al., 1994b), while those at the tips of the inhibitor, O26 and O76, accept hydrogen bonds from the amides of Thr31 and Thr131. Amino acid amide sites are identified by number. The color code is as follows: hydrogen is white, carbon is green, nitrogen is blue, protease or inhibitor oxygen is red, and water oxygen is yellow.

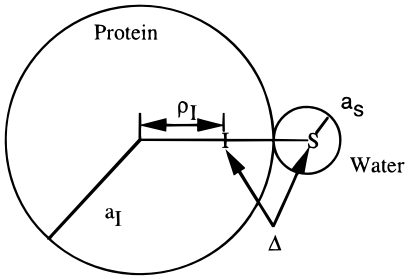

FIGURE 3: Schematic drawing illustrating features of the Ayant eccentric diffusion model (Ayant et al., 1977). The protein and water molecules are modeled as spheres, with radii a_I and a_S, respectively, undergoing translational and rotational diffusion. The distance between the center of the protein and the protein spin, *I*, is ρ_I, while the water spin, *S*, is assumed to be at the center of the water molecule. The distance of closest approach between the two spins is Δ.

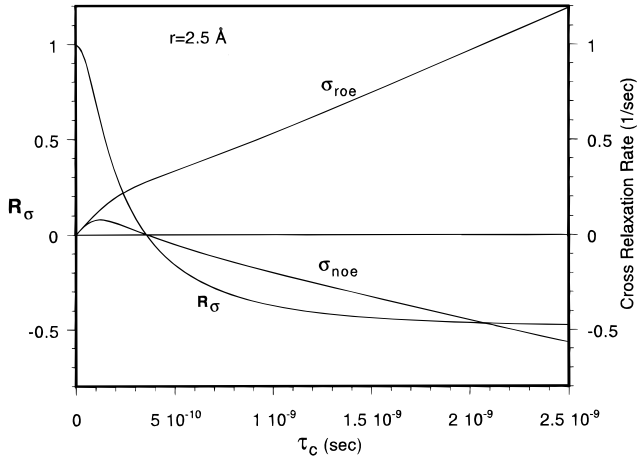

FIGURE 4: Cross relaxation rates, σ_{NOE} and σ_{ROE}, and their ratio, R_σ, plotted as a function of τ_c with an internuclear distance $r = 2.5$ Å, calculated using eqs 4 and 5, and the spectral density function of the exchange model, eq 6.

calculated using eqs 4, 5, and 7, are plotted against τ_{int}, for a range of values of S^2 and $\tau_c = 9.4$ ns, the rotational correlation time of the complex (Nicholson et al., 1995) (Figure 6). Internal motion has little effect on R_σ when S^2 is close to unity (not shown), for all values of τ_{int}. However, for $S^2 < 0.5$ the effect of internal motion on R_σ is significant, always increasing R_σ, since internal motion always reduces the effective correlation time.

Values of σ_{NOE}, σ_{ROE}, and R_σ, calculated using the Ayant model, are plotted as a function of D^{tr}, for Δ in the range 2.5−5.0 Å (Figure 7). Although the plots are in some ways similar to those in Figure 4, significant differences are also seen. To begin with, in the Ayant model R_σ depends upon the distance of closest approach of the protein and water spins, Δ. Furthermore, σ_{NOE} has a complex dependence upon Δ, except in the fast and slow motion limits. It is interesting that, in the fast and slow motion limits, σ_{NOE} and σ_{ROE} are approximately proportional to Δ^{-1}, a result in marked contrast with the r^{-6} dependence predicted by the exchange model, eq 6, and the Lipari and Szabo model, eq 7. Scaling arguments have been used (Brüschweiler & Wright, 1994) to show that an r^{-1} dependence is expected for dipolar relaxation in the diffusion model in the fast motion limit.

A final interesting difference between the relaxation rates calculated using the Ayant and exchange models is that the zero crossing of σ_{NOE} depends upon Δ (in the Ayant model) but not upon r (in the exchange model). This is because the correlation time in the diffusion model is proportional to Δ^2, and the zero crossing of σ_{NOE} occurs at an approximately constant value of $\omega_0\tau$ (approximately equal to 0.93) where τ is defined as Δ^2/D (Ayant et al., 1977). At

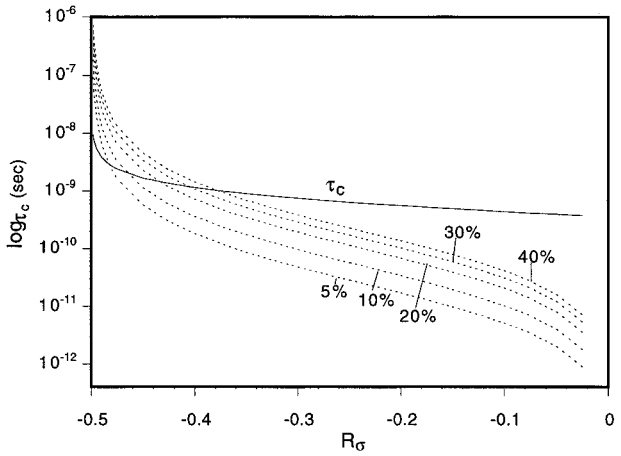

FIGURE 5: Correlation time, τ_c (solid line), and the error in τ_c (dotted lines) calculated using the exchange model and plotted as a function of R_σ. The assumed percent error in R_σ is indicated on each dotted line.

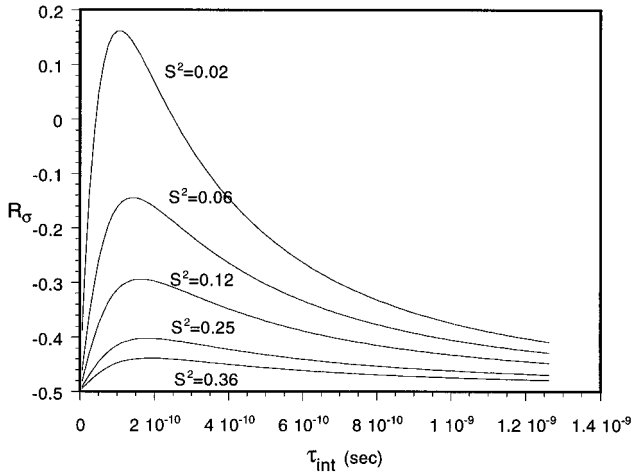

FIGURE 6: Plots illustrating the effect of internal motion upon R_σ. R_σ was calculated using the Lipari and Szabo (1982) spectral density function, eq 7, assuming that τ_c equals 9.4 ns, and is plotted as a function of the internal correlation time, τ_{int}, for various values of the generalized order parameter S^2. Note that S^2 ca. 0.12 corresponds to the internuclear vector wobbling in a cone having semiangle $\theta = 55°$.

500 MHz, $\tau \approx 300$ ps, close to the value of τ_c at which σ_{NOE} vanishes in the exchange model.

RESULTS

WROESY/WNOESY Spectra of Amide Protons. The amide cross peaks observed in the WROESY and WNOESY difference spectra and in the WNOESY sum spectrum are shown in Figure 8. For reasons discussed earlier, the WNOESY difference spectrum has slightly better sensitivity than the WROESY difference spectrum. In addition, the intensities of the cross peaks in the latter spectrum are both positive and negative, whereas in the former they are all positive. We interpret these data considering three mechanisms (Otting & Liepinsh, 1995) that can give rise to cross peaks in the difference spectra: (A) a direct NOE/ROE between a protein proton and a water proton, (B) a direct NOE/ROE between a protein proton and a labile proton that exchanges with water, and (C) chemical exchange of a protein proton with water. In mechanism B the exchange rate of the labile protein (or inhibitor) proton with water need only be a few times larger than 0.02 s^{-1}, the smallest NOE cross relaxation rate we detect, to yield observable cross peaks.

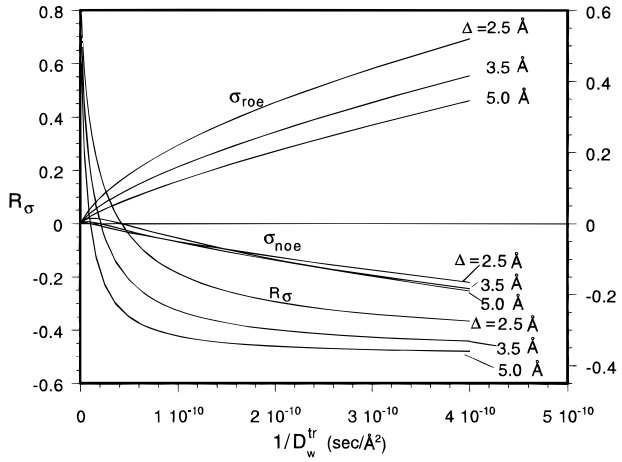

FIGURE 7: Comparison of σ_{NOE}, σ_{ROE} and R_σ calculated as a function of D_w^{tr} using the Ayant model (Ayant et al., 1977). In the simulation, the rotational diffusion coefficient is 9.4 ns, the sum of the radii of the protein and water spheres is 25 Å, the water spin is located at the center of the water sphere, the distance of closest approach between the protein and water spins, Δ, ranges from 2.5 to 5.0 Å, and $D \approx D_w^{tr}$, i.e., the translational diffusion coefficient of water is assumed to be much greater than that of the complex. The first 40 terms in eq 8 were used to calculate the spectral density functions, providing cross relaxation rates with an accuracy of better than 1%.

According to eq 5, σ_{ROE} is always positive. This implies that a cross peak in the WROESY spectrum is negative (Ernst et al., 1987) when either a class A or a class B mechanism is operative. Conversely, a positive WROESY cross peak implies that the dominant mechanism is direct exchange of the amide proton with water, class C. Twelve backbone amides have positive WROESY cross peaks (Figure 8a) and are assigned class C (Table 1). Hydrogen−deuterium exchange measurements (Yamazaki et al., 1996) have shown that these amides have exchange rates greater than 0.01 s^{-1}, consistent with this assignment. Intense class C cross peaks are also observed for the side chains of Arg residues but not for the side chains of Gln and Asn, in accord with their relative exchange rates measured in peptides at pH 5.2 (Wüthrich, 1986).

Unlike class C cross peaks, class B cross peaks cannot easily be distinguished from class A cross peaks using relaxation data. This distinction can sometimes be made using structural data in the following manner. The ROESY cross peaks having negative intensity in Figure 8a are all initially classified as A or B. Hydrogen−deuterium exchange data confirm this classification, because nearly all amides having negative cross peaks in Figure 8a have exchange rates with water that are less than 0.005 s^{-1} (Yamazaki et al., 1996). As indicated in Table 1, the backbone amide protons of Leu23, Gln18, and Arg87 are at least 4.5 Å from all labile protons (labile amine, carboxyl, hydroxyl, guanidino) in the protein and DMP323 molecules. Hence, these cross peaks are classified as type A because they are well isolated from labile protons. The remaining cross peaks are classified as type A/B since the amide protons are within 4.5 Å of either a labile protein proton or a labile DMP323 proton. Below we will discuss further the possibility of distinguishing type A and B cross peaks.

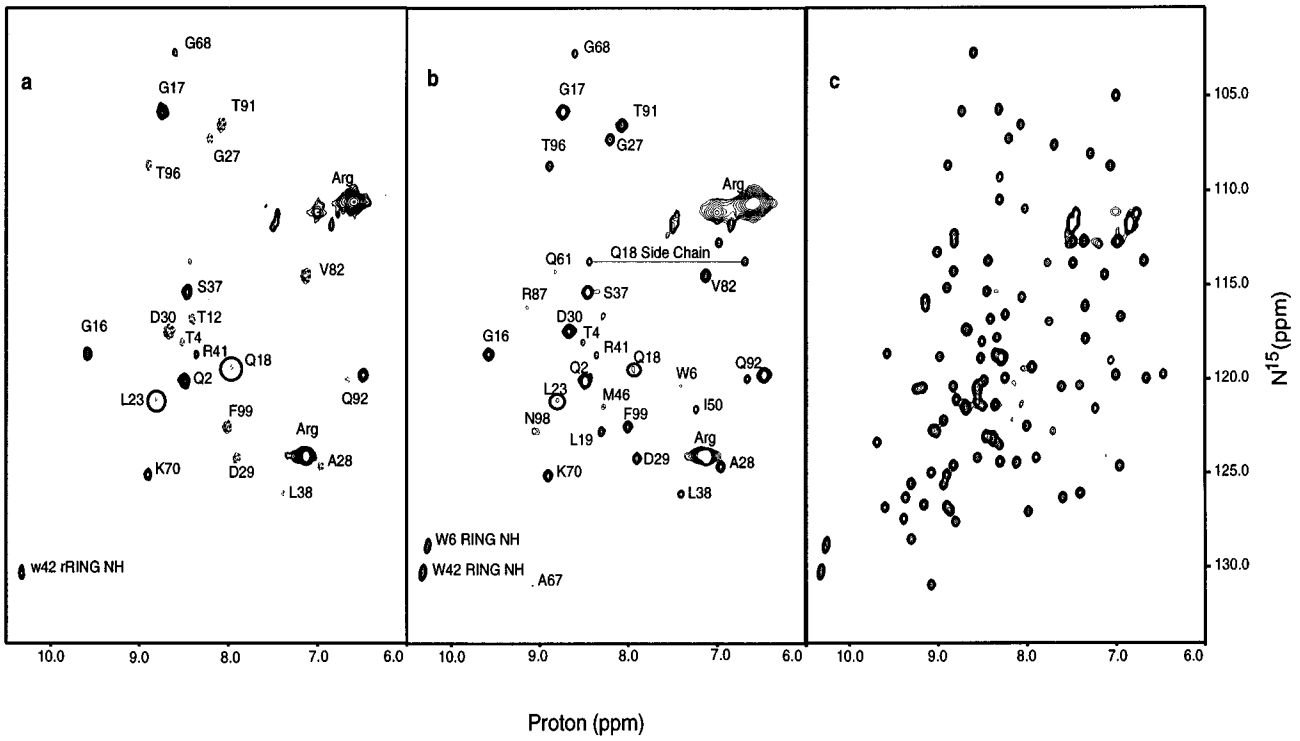

FIGURE 8: Comparison of the amide regions of the WROESY difference spectrum (a), the WNOESY difference spectrum (b), and the reference (sum) spectrum (c) of the HIV-1 protease/DMP323 complex. Type A cross peaks assigned to direct NOE/ROE interactions with crystalline water molecules are circled. The reference spectrum is plotted at a ca. 10-fold higher contour level than the WNOESY and WROESY difference spectra. A "control spectrum" (Grzesiek et al., 1994) shows that the weak I50 ROE in (b) is not with a water proton and is assigned to the DMP323 H201 proton at 4.94 ppm (Yamazaki et al., 1996).

WROESY/WNOESY Spectra of Aliphatic Protons. Cross peaks observed in the methyl region of the WROESY/WNOESY spectra of the protease/DMP323 complex are shown in Figure 9. Because only mechanisms A and B are possible for aliphatic protons, the sign of all ROESY cross peaks in the difference spectrum (Figure 9a) is opposite to that observed in the sum spectrum (not shown). [For technical reasons, related to the use of constant time evolution to remove carbon−carbon *J* couplings (Vuister & Bax, 1993), cross peaks of aliphatic carbons bonded to even and odd numbers of aliphatic carbons have opposite signs in both the difference and sum spectra; compare Figure 9b with Figure 9c]. Examination of Table 1 shows that ten of the aliphatic cross peaks are assigned to mechanism A by virtue of the fact that the aliphatic protons are at least 4.5 Å from the closest labile proton. The remaining cross peaks are classified as type A/B.

Most of the observed cross peaks listed in Table 1 are type A/B. Hence, it would be useful if the measured relaxation rates could be used to distinguish these mechanisms. To this end, we analyzed the values of σ_{NOE}, σ_{ROE}, and R_σ (Table 2), determined for the intense γ-methyl cross peaks of Thr4, -12, -74, -91, and -96 (Figure 9a,b). In the crystal structure, a water proton is observed within 3 Å of each Thr hydroxyl proton. We therefore first assume that NOE/ROE interactions with the hydration water molecules are solely responsible for the observed cross peaks. Applying the exchange model, eq 6, to the Thr relaxation data, we find correlation times in the range 0.7−0.75 ns and internuclear distances in the range 2.4−2.8 Å for the Thr hydration water molecules.

However, the crystal structure also shows that all five Thr γ-methyl protons are within 3.4 Å of the hydroxyl protons. The fact that we have not observed these hydroxyl protons distinct from the water resonance in NOESY spectra indicates that they are in fast chemical exchange with water. In contrast, Thr26, Thr31, and Thr80 hydroxyl protons were observed at 6.12, 5.95, and 4.61 ppm respectively, in a ^{15}N-separated 3D-NOESY spectrum, obtained with presaturation of the water signal (Yamazaki et al., 1996). This observation shows that their hydroxyl protons exchange slowly with water and explains the absence of cross peaks for residues Thr26 and Thr31 in Figure 9a,b. Cross peaks are observed for Thr80 because the chemical shift of its hydroxyl proton (4.61 ppm) is close to that of water (4.68 ppm), and the selective pulses used to align the water magnetization in the WNOESY/WROESY experiments align the magnetization of the Thr80 hydroxyl proton as well.

Because the exchange lifetime of every type of labile proton (Wüthrich, 1986) is much greater than the overall correlation time of the protein/DMP323 complex, $\tau_o = 9.4$ ns, we use the spectral density function given by eq 7 with $\tau_c = \tau_o = 9.4$ ns to analyze the cross relaxation rates. We reproduce the measured values of the Thr γ-methyl cross relaxation rates with $S^2 \approx 0.12$, $\tau_{int} \approx 100$ ps, and **r** in the range of 2.6−3.0 Å. This analysis underestimates the value of S^2 because it does not include changes in the length of **r** caused by internal motion (i.e., methyl or χ_1 rotomer hopping). For example, if **r** assumes two lengths that differ by ca. a factor of 2, the calculated value of S^2 increases to a value of ca. 0.2. This corresponds to motion of the internuclear vector in a cone having a semiangle of 55°, a value which is 5−10° larger than that found for mobile methyl groups of leucine residues in staphylococcal nuclease (Nicholson et al., 1992).

Table 1: Classifications of WNOESY/WROESY Cross Peaks, NH Exchange Rates, and Hydrogen Atom Solvent Accessibility, Listed Along with the Calculated Distances of the Closest Labile Proton and Closest Water Proton in the Protease/DMP323 Complex[a]

residue	proton	class[b]	NH exchange[c]	accessible[d]	labile nearby[e]	crystal water[f]
Pro1	H^{β}	B	NA	yes	Pro1-NH (3.5)	no
	H^{γ}	B	NA	yes	Pro1-NH (3.0)	no
	H^{δ}	A/B	NA	yes	Pro1-NH (2.2)	448 (3.9)
Gln2	NH	C	fast	yes		486 ((3.4))
Val3	$H^{\gamma 1}$	A	NA	no		471 ((2.4))
	$H^{\gamma 2}$	A/B	NA	yes	Pro1H^{r} (4.5)	445 (2.7)
Thr4	H^{γ}	A/B	NA	yes	Thr4$H^{\gamma 1}$ (3.4)	408 (3.2)
Trp6	NH	C	Fast	No		403 (3.3)
	H^{ϵ}	C	fast	yes		403 (3.3)
Arg8	NH	C	fast	yes		458 ((2.7))
Thr12	NH	A/B	fast	no	Thr12$H^{\gamma 1}$ (2.7)	497 (1.8)
	H^{γ}	A/B	NA	yes	Thr12$H^{\gamma 1}$ (3.1)	450 ((2.9))
Lys14	H^{γ}	A/B	NA	yes	Gly17-NH (3.1)	476 (2.8)
	H^{δ}	A/B	NA	no	Lys14H^{ξ} (2.4)	454 ((2.6))
	H^{ϵ}	A/B	NA	yes	Lys14H^{ξ} (2.1)	454 ((2.5))
Gly16	NH	C	fast	yes		405/437 (2.2)
Gly17	NH	C	fast	yes		437 (1.2)
Gln18	NH	A	slow	no		437 ((3.8))
Leu19	$H^{\delta 1}$	A	NA	yes		451 ((4.3))[g]
Lys20	H^{δ}	A	NA	no		438 (3.2)[g]
	H^{ϵ}	A/B	NA	no	Lys20H^{ξ} (2.2)	493 (2.3)
Leu23	NH	A	slow	no		no
	$H^{\delta 1}$	A/B	NA	yes	Arg8H^{η} (3.2)	401 (3.7)[g]
	$H^{\delta 2}$	A	NA	no		401 (2.6)[g]
Gly27	NH	B	slow	no	DMP-HO4 (3.3)	no
Ala 28	NH	A/B	slow	no	DMP-HO4 (3.2)	401 ((3.3))
	H^{β}	A/B	NA	no	DMP-OH4 (3.8)	456 (3.9)
Asp29	NH	A/B	fast[c]	no	DMP-HO27 (3.2)	456 (2.2)
	H^{β}	A/B	NA	no	DMP-HO27 (3.6)	502 (2.2)[h]
Asp30	NH	A/B	slow	no	DMP-HO27 (2.0)	456 (4.1)
Met36	H^{ϵ}	A/B	NA	no	Lys20H^{ξ} (2.6)	479 ((4.0))
Ser37	NH	C	fast	yes	Ser37H^{γ} (4.1)	411 ((2.2))
	$H^{\beta 1}$	A/B	NA	yes	Ser37H^{γ} (3.0)	435 ((2.1))
	$H^{\beta 2}$	A/B	NA	yes	Ser37H^{γ} (3.1)	411 ((3.3))
Leu 38	NH	A/B	fast	no	Ser37H^{γ} (3.9)	509 (2.3)
Arg41	NH	A/B	fast	yes		498 ((3.1))
	H^{β}	A/B	NA	yes	Trp42-NH (3.1)	498 ((4.0))
	H^{δ}	A/B	NA	yes	Asp60-NH (4.2)	426 ((2.2))
Trp42	H^{ϵ}	C	fast	yes		421 ((2.3))
Lys43	H^{ϵ}	A/B	NA	yes	Lys43H^{ξ} (2.2)	489 (2.6)
Lys45	H^{γ}	A/B	NA	yes	Lys45H^{ξ} (2.6)	470 ((2.2))
	H^{ϵ}	A/B	NA	yes	Lys45H^{ξ} (2.3)	470 ((2.2))
Met46	NH	C	fast	yes		no
Ile47	$H^{\gamma m}$	A/B	NA	no	Lys45H^{ξ} (3.3)	452 (1.9)
	H^{δ}	A/B	NA	no	DMP-OH27 (4.2)	452 (3.3)
Ile50	$H^{\gamma m}$	A/B	NA	no	Thr180$H^{\gamma 1}$ (4.2)	478 ((3.6))
	H^{δ}	B	NA	no	Thr180$H^{\gamma 1}$ (2.9)	no
Lys55	H^{ϵ}	A/B	NA	yes	Lys55H^{ξ} (2.2)	505 ((3.8))
Gln61	NH	C	fast	yes		459 ((2.2))
Ile63	$H^{\delta 2}$	A	NA	yes		454 ((3.3))
Ala67	H^{β}	A/B	NA	yes	His69H^{δ} (2.1)	497 (3.9)
Gly68	NH	C	fast	yes		no
Lys70	NH	C	fast	no		427 (1.4)
	H^{ϵ}	A/B	NA	yes	Lys70H^{ξ} (2.3)	427 (2.9)
Thr74	NH	A/B	fast	no	Thr74$H^{\gamma 1}$ (3.2)	402 ((1.0))
	H^{γ}	A/B	NA	yes	Thr74$H^{\gamma 1}$ (2.8)	459 ((2.1))
Val75	$H^{\gamma 1}$, $H^{\gamma 2}$	A	NA	no		no
Leu76	H^{β}	A	NA	no		477 (3.3)
	$H^{\delta 1}$	A	NA	no		477 (2.3)
	$H^{\delta 2}$	A/B	NA	no	DMP-HO27 (4.1)	477 (2.9)
Val77	$H^{\gamma 1}$	A/B	NA	no	Arg57H^{η} (1.9)	479 ((3.5))
	$H^{\gamma 2}$	B	NA	no	Arg57H^{η} (3.6)	no
Thr80	H^{γ}	A/B	NA	no	Thr80H^{γ} (3.1)	474 ((4.1))
Val82	$H^{\gamma 1}$	A	NA	yes		503 (2.0)[g,h]
	$H^{\gamma 2}$	A/B	NA	no	Thr80H^{γ} (2.7)	491 ((3.8))
Ile84	$H^{\gamma m}$	B	NA	no	Thr80$H^{\gamma 1}$ (3.9)	no
	H^{δ}	B	NA	no	Thr80H^{γ} (3.6)	no
Arg87	NH	A	slow	no		420 ((4.2))
Thr91	NH	A/B	slow	no	Thr91$H^{\gamma 1}$ (2.0)	416 (4.4)
	H^{β}	A/B	NA	no	Thr91$H^{\gamma 1}$ (2.6)	425 (3.7)
	H^{γ}	A/B	NA	no	Thr91$H^{\gamma 1}$ (3.0)	406 (2.3)
Gln92	NH	A/B	fast	yes	Thr91$H^{\gamma 1}$ (2.2)	424 (3.9)
Ile93	H^{δ}	B	NA	no	His69H^{δ} (3.2)	no

Table 1 (Continued)

residue	proton	class[b]	NH exchange[c]	accessible[d]	labile nearby[e]	crystal water[f]
Ala95	$H^{\beta i}$	A	NA	no		403 ((4.3))[j]
Thr96	NH	A/B	slow	no	Thr96$H^{\gamma 1}$ (4.1)	431 ((4.1))
	H^{γ}	A/B	NA	yes	Thr96H^{γ} (3.3)	431 (2.3)
Asn98	H^{β}	A/B	NA	no	Thr196$H^{\gamma 1}$ (2.1)	522 (2.1)
Phe99	NH	A/B	slow	no	Pro101H^{r} (2.6)	486 (3.2)[h]

[a] Each protease monomer contains 99 residues, numbered 1−99 and 101−199. Because the average structure of the protease/DMP323 complex is C_2 symmetric in solution, residues *i* and *i* + 100 have identical chemical shifts and cannot be distinguished in NMR spectra. Therefore, an NMR cross peak assigned to residue *i* is also assigned to residue *i* + 100. Interproton distances were calculated by building hydrogen atoms onto the heavy atoms of protein and water molecules in the protease/DMP323 crystal structure using the X-PLOR protocol (Brünger, 1987). Because of uncertainties in the orientation of the water molecules and in the water oxygen atom coordinates, the distances in the last column have estimated average uncertainties of ca. 1 Å. [b] Cross peak classification is described in Results. [c] Proton exchange rates determined by NH−D exchange experiments. "Slow" indicates that the lifetime of the amide proton is longer than ca. 5 min. "Fast" indicates that the lifetime is shorter than ca. 3 min. In the case of Asp29, the NH signal is not attenuated by presaturation of the water peak, indicating that its exchange lifetime is at least several seconds. NA means "not applicable". [d] Determined using Quanta software by rolling a sphere of 1.4 Å radius over the surface of the crystal structure of the protease/DMP323 complex. [e] The labile proton within 4.5 Å of the proton listed in the second column. Only the closest labile proton is listed. Note that Gly17NH is listed as the labile proton because of its rapid H−D exchange (Yamazaki et al., 1994a) and its σ_{ROE} value is negative. The side chain amides of Asn and Gln exchange with solvent at a slow rate, ca. 2×10^{-3} s^{-1} at pH 5.2 (Wüthrich, 1986), and we did not detect significant exchange cross peaks between water and the side chains of either Asn or Gln residues in WNOESY/WROESY spectra (Figure 8). Therefore, the side chain amides of Asn and Gln are not classified as labile protons for the purpose of this study. [f] The distance of the closest water proton, located within 4.5 Å of the proton in column 2, is listed in angstroms. The distance is listed within a single set of parentheses when the closest protein proton is in monomer 1 (residue *i*) and is listed within double parentheses when the closest proton is in monomer 2 (residue *i* + 100). Not all water molecules have symmetry-related partners in the crystal structure, as seen in Figure 2. For type A cross peaks, the proton of the next nearest water is either further than 4.5 Å or at least 2 Å more distant than the proton listed. [g] A C_2 symmetry-related water molecule is not seen in the crystal structure. [h] Electron density is weak. [i] Overlap with Thr80H^{γ}. [j] Water 403 is near Ala195H^{β}. There is no water within 4.5 Å near Ala95H^{β} in the crystal structure.

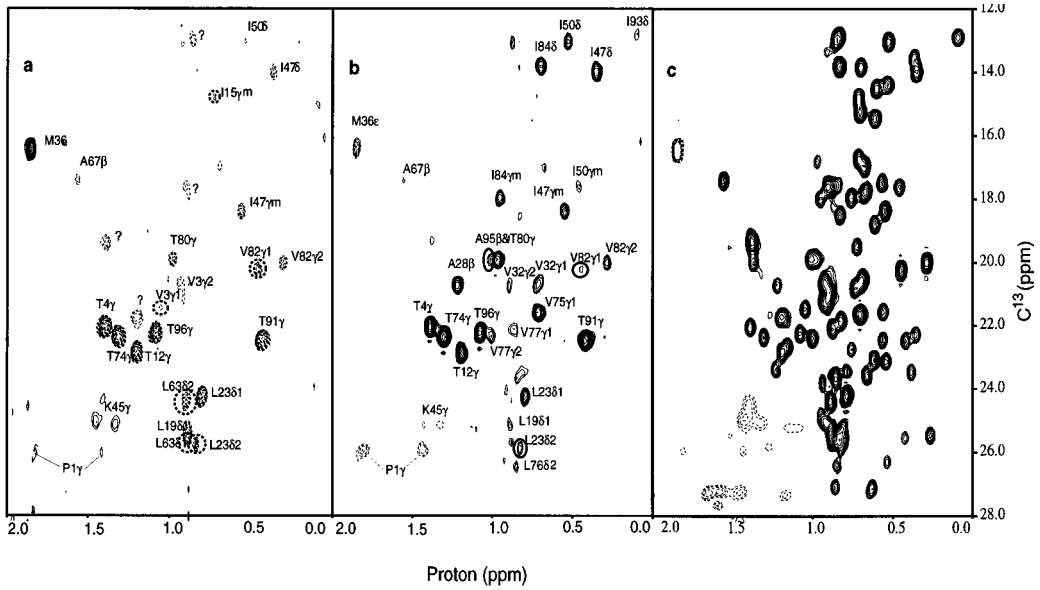

FIGURE 9: Comparison of the methyl regions of the WROESY difference spectrum (a), the WNOESY difference spectrum (b), and the reference (sum) spectrum (c) of the HIV-1 protease/DMP323 complex. Type A cross peaks, assigned to direct NOE/ROE interactions with crystalline water molecules are circled, and cross peaks labeled with the question mark are from degraded protease. The reference spectrum is plotted at a ca. 10-fold higher contour level than the WNOESY and WROESY difference spectra.

In summary, it is possible to reproduce the observed cross relaxation rates for the Thr γ-methyl groups using either model A or model B with physically reasonable parameters. This statement applies to the other type A/B cross peaks. Hence, we are not able to distinguish a type A from a type B mechanism, when both a hydration water proton and a labile protein proton are within ca. 4.5 Å of the proton having a WNOESY/WROESY cross peak.

Finally, we note that predictions of the Ayant model were inconsistent with the data, unless we employed a value for *D* that was at least an order of magnitude smaller than that of bulk water. Comparison of the results plotted in Figure 7 with those in Table 2 shows that the Ayant model predicts the wrong sign for σ_{NOE} and/or values of σ_{ROE} that are much smaller than the observed values, when $D \approx D_w^{tr}$.

DISCUSSION

Analysis of Type A Cross Peaks. The type A cross peaks, circled in Figures 8 and 9, are weak, indicating that the correlation times of the hydration water molecules are short and/or the water−protein interproton distances are large. Due to their weak signal intensities, the only type A cross peaks for which we were able to obtain values of both σ_{NOE} and σ_{ROE} were Lys20H^{δ}/water 438, Leu23$H^{\delta 2}$/water 401, and Val82$^{\gamma 1}$/water 503 (Tables 1 and 2). The experimental cross relaxation rates, together with eqs 4−6, yield residence times for waters 438, 401, and 503 of 530, 520, and 460 ps, respectively, and distances between the Leu and Val methyl

Table 2: Fractional WNOESY/WROESY Difference Intensities, ξ, Proton Spin Flip Rates,[a] ϱ_1, Rotating Frame Relaxation Rates, ϱ_2, Cross Relaxation Rates, σ_{NOE} and σ_{ROE}, Cross Relaxation Rate Ratios, $R_\sigma = \sigma_{NOE}/\sigma_{ROE}$, and Rotational Correlation Times,[b] τ_c

proton	ξ_{NOE}	ξ_{ROE}	$\varrho_1 + k_n$	$\varrho_2 + k_r$	σ_{NOE}	σ_{ROE}	R_σ	τ_c
Pro1H$^{\delta}$	1.3E−01	−1.80	1.5	6.1	−1.90	20.65	−0.09	4.3E−10
Lys14H$^{\delta}$	1.6E−02	−2.0E−01	8.2	36.8	−0.31	1.65	−0.19	5.4E−10
Leu23H$^{\delta1}$	3.7E−03	−2.0E−02	2.4	5.8	−0.05	0.41	−0.12	4.6E−10
Asp29H$^{\beta}$	6.6E−03	−0.22	5.8	28.6	−1.04	2.35	−0.44	1.5E−09
Met36H$^{\epsilon}$	1.5E−03	−9.3E−03	2.8	9.4	−0.02	0.17	−0.13	4.7E−09
Ser37H$^{\beta1}$	3.3E−02	−4.9E−01	7.7	30.8	−0.64	4.90	−0.13	4.7E−10
Ser37H$^{\beta2}$	3.5E−02	−4.7E−01	8.4	(33.6)[c]	−0.70	4.3	−0.16	5.0E−10
Arg41H$^{\beta}$	2.2E−03	−9.8E−03	5.6	22.2	−0.04	0.13	−0.33	8.3E−10
Ile47H$^{\gamma}$	5.7E−03	−3.0E−02	7.4	29.6	−0.11	0.31	−0.35	9.0E−10
Ile47H$^{\delta}$	9.8E−03	−2.4E−02	6.9	30.5	−0.18	0.24	−0.75	
Ile50H$^{\gamma}$	4.7E−03		13.1	45.3	−0.12			
Ile50H$^{\delta}$	5.8E−03		7.1	27.4	−0.11	0.15		
Lys55H$^{\epsilon}$	1.5E−02	−7.9E−02	4.2	13.7	−0.23	1.30	−0.18	5.3E−10
Leu76H$^{\beta}$	2.4E−03	−1.7E−02	5.8	28.4	−0.05	0.18	−0.27	6.8E−10
Leu76H$^{\delta2}$	9.8E−03		3.0	20.4	−0.13			
Val77H$^{\gamma1}$	3.6E−02		8.3	36.5	−0.68			
Val77H$^{\gamma2}$	3.5E−03		10.0	37.9	−0.08			
Val82H$^{\gamma2}$	2.2E−03	−1.0E−02	7.5	16.4	−0.04	0.15	−0.27	6.8E−10
Ile84H$^{\gamma m}$	1.0E−02		8.3	37.6	−0.68			
Ile84H$^{\delta}$	1.2E−02		8.7	24.3	−0.24			
Ile93H$^{\delta}$	4.0E−03		7.1	36.1	−0.08			
Thr4H$^{\gamma2}$	3.6E−02	−1.8E−01	6.6	24.8	−0.62	2.20	−0.28	7.0E−10
Thr12H$^{\gamma2}$	1.7E−02	−1.0E−01	7.2	26.9	−0.31	1.12	−0.27	6.8E−10
Thr74H$^{\gamma2}$	3.6E−02	−3.0E−01	10.7	34.4	−0.76	2.70	−0.28	7.0E−10
Thr91H$^{\gamma2}$	4.5E−02	−3.6E−01	9.3	37.5	−0.88	2.90	−0.30	7.5E−10
Thr96H$^{\gamma2}$	3.3E−02	−1.9E−01	8.1	28.5	−0.61	2.04	−0.30	7.5E−09
Lys20H$^{\delta}$	8.1E−03	−6.9E−02	7.2	23.7	−0.15	0.85	−0.18	5.3E−10
Val3H$^{\gamma1}$	<7.2E−04	1.2E−02	7.4	26.8	>−0.016	0.16	>0.1	∼4E−10
Leu23H$^{\delta2}$	2.2E−02	−7.8E−02	1.0	5.2	−0.27	1.62	−0.17	5.2E−10
Leu63H$^{\delta2}$	<1.8E−04	−3.7E−03	5.8	15.8	<−0.04	0.06		∼4E−10
Leu76H$^{\delta1}$	5.5E−03	<4.3E−03	9.9	30.6	−0.12			
Val82H$^{\gamma1}$	1.1E−03	−1.2E−02	8.1	18.1	−0.02	0.17	−0.12	4.6E−10

[a] All rates are in s^{-1}. Note that $\sigma_{NOE} = -k_n$ and $\sigma_{ROE} = -k_r$, as defined previously (Grzesiek & Bax, 1993b). The table contains three sections: the first contains class A/B cross peak data; the second contains threonine data; the third contains class A cross peak data. For class A cross peaks seen only in the WROESY difference spectrum (and not in the WNOESY difference spectrum, presumably because σ_{NOE} is near its zero crossing, Figure 4), ξ_{NOE} is the upper limit estimated from the rms noise. The Leu76H$^{\delta2}$ cross peak is seen in the WNOESY but not in the WROESY difference spectrum, presumably because the latter spectrum is less sensitive (see Theoretical Background). The A95H$^{\beta}$ class A cross peak is not included in the table because it overlaps with Thr80H$^{\gamma}$. [b] In seconds, calculated using eqs 3−5. [c] Approximate value calculated assuming that $\varrho_2 - \sigma_{ROE} = 4(\varrho_1 - \sigma_{NOE})$.

protons and the water protons of 2.6 and 3.8 Å, respectively. These distances are reasonable because we expect to observe ROESY cross peaks only for internuclear separations less than ca. 3.5 Å, because of signal-to-noise-ratio limitations.

For 11 of the type A cross peaks, protein protons are within 4.5 Å of crystalline water protons (Table 1). The Leu23H$^{\delta2}$ cross peaks are assigned to an NOE/ROE interaction with water 401 (Table 1), a nearly buried water that accepts a hydrogen bond from the side chain amide of Arg187 and donates a hydrogen bond to the carbonyl oxygen of Thr126. A symmetry-related water molecule is not observed in the crystal structure (Figure 2) because the Arg87 side chain occupies the position expected of the related water molecule. As noted in the previous paragraph, the correlation time for water 401 is ca. 500 ps, showing that, in contrast with water 301 (Grzesiek et al., 1994), it is not tightly bound to the complex. It is possible that there is a dynamic equilibrium in solution, involving both types of conformations seen in the crystal.

The type A Leu76H$^{\delta2}$ cross peak is assigned to an interaction with water 477 (Table 1). Water 477 accepts a hydrogen bond from the amide of Thr31. Although the distances between the water 477 protons and the Thr31NH and Leu76H$^{\delta1}$ protons are less than 2.5 Å in the crystal structure, ROE cross peaks are not observed in either the amide or methyl difference spectra. In addition, the NOE cross peak of Leu76H$^{\delta1}$ protons is weak. Taken together, these observations suggest that the residence time of water 477 is less than a few hundred picoseconds. The same conclusion applies to the symmetry-related water 415 (Figure 2).

The class A cross peaks of Gln118NH, and Leu119H$^{\delta1}$ are assigned to waters 437 and 451, respectively (Table 1). Although these two water molecules are located on the surface of the protein, they hydrogen bond to the protein, which presumably increases their residence times sufficiently, $\tau_{re} > 360$ ps, so that their cross peaks are observed.

With the exception of water 403, none of the remaining water molecules that are assigned to class A cross peaks, waters 403, 420, 454, 471, and 503 (Table 1), form hydrogen bonds with the protein in the crystal structure, and all are at least partially exposed to solvent water. Waters 403, 420, and 471 exhibit weak NOE but no ROE cross peaks, suggesting that they are loosely bound with residence times less than 500 ps. Waters 454 and 503 are virtually unique in that their NOE cross peaks, to Leu163 and Val182, respectively, are significantly smaller than their ROE cross peaks. This observation indicates that $|R_\sigma| \ll 1$; i.e., their

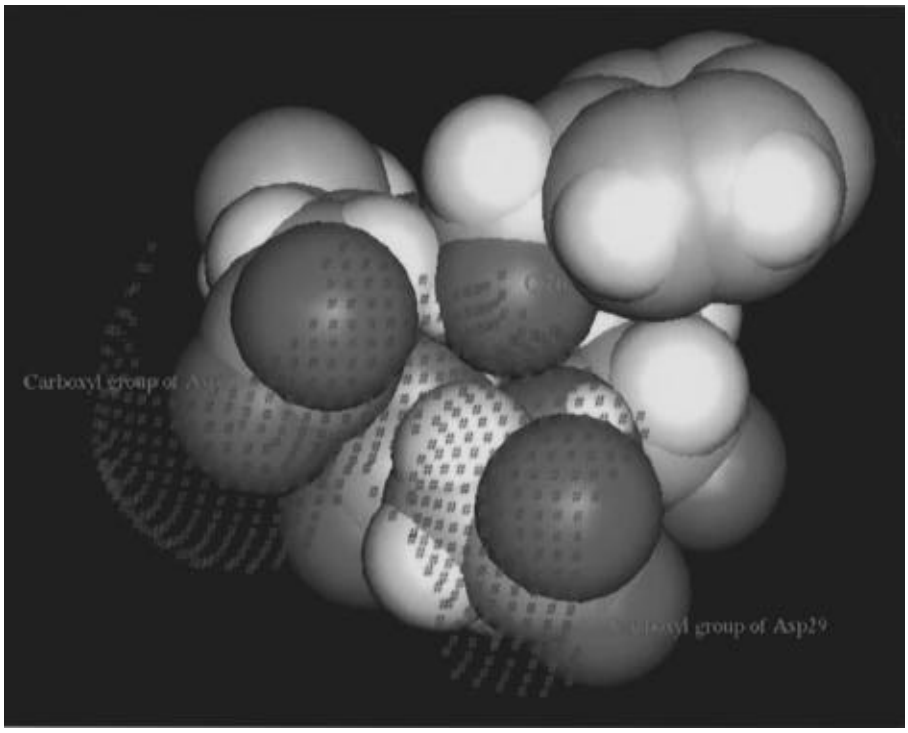

FIGURE 10: Quanta drawing of the HIV protease/DMP323 complex in the neighborhood of the DMP323 O26 hydroxyl oxygen, the red atom in the center of the drawing. The solvent-exposed surface is spotted green "#", and the atom types are color coded as follows: hydrogen is white, carbon is green, nitrogen is blue, and oxygen is red.

residence times are ca. 400 ps (Figure 4). It may be recalled that the cross relaxation rates together with eqs 3−5 yielded a residence time of 460 ps for water 503.

Crystal hydration water molecules have not been assigned to type A cross peaks of Leu23NH and Val75H$^{\gamma}$, because the protons of these residues are not found within 4.5 Å of water protons in the crystal structure. While the Leu23NH and Val75H$^{\gamma}$ protons are buried, they are respectively within 2 and 4 Å of the protein surface, suggesting that their weak cross peaks are due to NOE interactions with poorly ordered surface water molecules that are not seen in the crystal structure.

Water Molecules Near the Protease/Inhibitor Interface. Water molecules 422/456, 430/480 (the slash indicates symmetry-related waters), and 452 are at the protease/inhibitor interface in the crystal structure (Figure 2). Protons of the waters 430/480 are within 2.5 Å of the Gly48/148 amide protons, but neither NOE nor ROE cross peaks are observed, indicating that the residence times are very short or that the internuclear distances are much greater than 2.5 Å in solution. Although water 453/Ile47H$^{\gamma}$/H$^{\delta}$ and water 422/456/AspNH29/129 cross peaks are observed, the Ile47 methyl and Asp29/129 amide protons are within 4.5 Å of labile protons (Table 1), precluding quantitative analysis of the data. However, the Asp29 cross peak is one of the stronger cross peaks observed in the WROESY spectrum (Figure 8a). Furthermore, waters 422/456 are buried and accept hydrogen bonds from the amides of Asp29/129. Taken together, these results suggest that waters 422/456 may have a structural role in the complex that should be considered in the design of future cyclic urea inhibitors.

Highly Mobile Water Molecules. Many of the water molecules at the protein surface in the crystal structure are not seen by NMR. It has been noted (Brüschweiler & Wright, 1994) that water molecules undergoing diffusive jumps on a lattice are X-ray observable. In solution, such water molecules would undergo rapid continuous diffusion, and their cross relaxation rates can be estimated using the Ayant model. Assuming that the solvent translational diffusion coefficient is that of bulk water, the predicted values of σ_{NOE} and σ_{ROE} are less than 0.02 s^{-1} for $\Delta \geq 2.5$. Even if the diffusion coefficient is reduced 10-fold, $\sigma_{NOE} < 0.02$ s^{-1} for $\Delta \geq 2.5$. The signal intensity in the WNOESY or WROESY experiment is proportional to the value of σ_{NOE} or σ_{ROE} (see eqs 2 and 3), and we have not observed cross peaks having σ_{NOE} or σ_{ROE} values less than 0.02 or 0.06, respectively. Hence, these results indicate that cross peaks of water molecules undergoing rapid diffusion are too weak to detect, at least for a large protein at a concentration below 2 mM. Cross peaks due to highly mobile hydration water molecules are observed for the peptide oxytocin (Otting et al., 1991), at a concentration of ca. 50 mM.

Flexibility at the Protein/DMP323 Interface. We recognized that one potential problem with locating bound water molecules at the protease/inhibitor interface was the possibility that the four hydroxyl protons of DMP323 were in fast exchange with water. This would make it difficult to assign a cross peak to a unique mechanism (as discussed earlier for waters 422/456). However, the observation that the hydroxyl protons of Thr26, Thr31, and Thr80 were in slow exchange with solvent water suggested that the same might be true for the hydroxyl protons of DMP323. The inhibitor hydroxyl groups were designed to hydrogen bond to the complementary P1/P2 sites in the protein, and such hydrogen bonds are observed in the crystal structure. However, our NMR results indicate that rapid exchange with solvent causes all the hydroxyl protons of DMP323 to resonate at the water signal.

The exchange of the H27/H77 hydroxyl protons with solvent can be explained by the fact that these hydroxyl

groups are partially accessible to water (Figure 10). In contrast, the H4/H5 hydroxyl groups are completely buried and form a network of hydrogen bonds with the protease catalytic Asp25/125 side chains (Yamazaki et al., 1994b). Because DMP323 is a potent inhibitor with a K_i of 0.27 nM, it is not likely that dissociation of the protease/DMP323 complex causes the solvent exchange of the H4/H5 hydroxyl protons. $^1H-^{15}N$ HSQC spectra of the protease/epi-KNI-272 complex, where epi-KNI-272 is an asymmetric inhibitor with a K_i of ca. 1 nM (Baldwin et al., 1995), show distinct cross peaks for residues i and $i + 100$, with no evidence of exchange broadening, at 45 °C. This observation indicates that the dissociation rate constant for DMP323 at 34 °C is less than 1 s^{-1}. This rate is much too small to average the chemical shifts of the H4/H5 hydroxyl and bulk water signals, unless the intrinsic H4/H5 chemical shift accidentally coincides with that of bulk water. We therefore ascribe the solvent exchange of the inhibitor hydroxyl protons to local fluctuations of the protease/DMP323 complex that allow solvent molecules to penetrate into the inhibitor binding site. This conclusion is supported by the observation (Yamazaki et al., 1994b) that the carboxyl protons of the catalytic Asp25/125 residues, though buried and hydrogen bonded to the H4/H5 hydroxyls, undergo H−D exchange with solvent, as evidenced by the fact that a single exchange-averaged Asp C^γ chemical shift is seen in 50% deuterated water. Hence, while the binding site of the protease/DMP323 complex is highly ordered, it nonetheless appears to be flexible on the millisecond to microsecond time scale.

ACKNOWLEDGMENT

We thank Frank Delaglio and Dan Garrett for providing NMR data analysis software, Rolf Tschudin for expert technical support, and Ann Frances Miller for critically reading the manuscript.

REFERENCES

Abragam, A. (1961) *The Principles of Nuclear Magnetism*, p 300, Oxford University Press, Oxford.

Ayant, Y., Belorizky, E., Fries, P., & Rosset, J. (1977) *J. Phys. 38*, 325−337.

Baldwin, E. T., Bhat, T. N., Gulnik, S., Liu, B., Topol, I. A., Kiso, Y., Mimoto, T., Mitsuya, H., & Erickson, J. W. (1995) *Structure 3*, 581−590.

Brünger, A. T. (1987) *X-PLOR, a System for X-Ray Crystallography and NMR*, Version 3.1, p 112, Yale University Press, New Haven and London.

Brüschweiler, R., & Wright, P. E. (1994) *Chem. Phys. Lett. 229*, 75−81.

Clore, G. M., Bax, A., Wingfield, P. T., & Gronenborn, A. M. (1990) *Biochemistry 29*, 5671−5676.

Delaglio, F., Grzesiek, S., Vuister, G. W., Zhu, G., Pfeifer, J., & Bax, A. (1995) *J. Biomol. NMR 6*, 277−293.

Ernst, R. R., Bodenhausen, G., & Wokaun, A. (1987) *Principles of Nuclear Magnetic Resonance in One and Two Dimensions*, Vol. 14, pp 519−527, Clarendon Press, Oxford.

Garrett, D. S., Powers, R., Gronenborn, A. M., & Clore, G. M. (1991) *J. Magn. Reson. 95*, 214−220.

Gillen, K. T., Douglass, D. C., & Hoch, M. J. R. (1972) *J. Chem. Phys. 57*, 5117−5119.

Grzesiek, S., & Bax, A. (1993a) *J. Am. Chem. Soc. 115*, 12593−12594.

Grzesiek, S., & Bax, A. (1993b) *J. Biomol. NMR 3*, 627−638.

Grzesiek, S., Bax, A., Nicholson, L. K., Yamazaki, T., Wingfield, P. T., Stahl, S. J., Eyermann, C. J., Torchia, D. A., Hodge, C. N., Lam, P. Y. S., Jadhav, P. K., & Chang, C.-H. (1994) *J. Am. Chem. Soc. 116*, 1581−1582.

Kriwacki, R. W., Hill, R. H. R., Flanagan, J. M., Caradonna, J. P., & Prestegard, J. H. (1993) *J. Am. Chem. Soc. 115*, 8907−8911.

Lam, P. Y., Jadhav, P. K., Eyermann, C. J., Hodge, C. N., Ru, Y., Bacheler, L. T., Meek, J. L., Otto, M. J., Rayner, M. M., Wong, Y. N., Chang, C.-H., Weber, P. C., Jackson, D. A., Sharpe, T. R., & Erickson-Viitanen, S. (1994) *Science 263*, 380−384.

Lipari, G., & Szabo, A. (1982) *J. Am. Chem. Soc. 104*, 4559−4570.

Nicholson, L. K., Kay, L. E., Baldisseri, D. M., Arango, J., Young, P. E., Bax, A., & Torchia, D. A. (1992) *Biochemistry 31*, 5253−5263.

Nicholson, L. K., Yamazaki, T., Torchia, D. A., Grzesiek, S., Bax, A., Kaufman, J. D., Stahl, S. J., Wingfield, P. T., Lam, P. Y. S., Jadhav, P. K., Hodge, C. N., Domaille, P. J., & Chang, C.-H (1995) *Nat. Struct. Biol. 2*, 274−280.

Otting, G., & Wüthrich, K. (1989) *J. Am. Chem. Soc. 111*, 1871−1875.

Otting, G., & Liepinsh, E. (1995) *Acc. Chem. Res. 28*, 171−177.

Otting, G., Liepinsh, E., & Wüthrich, K. (1991) *Science 254*, 974−980.

Vuister, G. W., & Bax, A. (1993) *J. Am. Chem. Soc 115*, 772−777.

Wlodawer, A., & Erickson, J. W. (1993) *Annu. Rev. Biochem. 62*, 543−585.

Wüthrich, K. (1986) *NMR of Proteins and Nucleic Acids*, pp 23−25 John Wiley & Sons, New York.

Yamazaki, T., Nicholson, L. K., Torchia, D. A., Stahl, S. J., Kaufman, J. D., Wingfield, P. T., Domaille, P. J., & Campbell-Burk, S. (1994a) *Eur. J. Biochem. 219*, 707−712.

Yamazaki, T., Nicholson, L. K., Wingfield, P. T., Stahl, S. J., Kaufman, J. D., Lam, P. Y. S., Ru, Y., Jadhav, P. K., Chang, C.-H., Weber, P. C., & Torchia, D. A. (1994b) *J. Am. Chem. Soc. 116*, 10791−10792.

Yamazaki, T., Hinck, A. P., Wang, Y.-X., Nicholson, L. K., Torchia, D. A., Wingfield, P. T., Stahl, S. J., Kaufman, J. D., Chang, C.-H., Domaille, P. J., & Lam, P. Y. S. (1996) *Protein Sci. 5*, 495−506.

BI9610764